Intersubband absorption in $In_{0.53}Ga_{0.47}As/In_{0.52}Al_{0.48}As$ multiple quantum wells

Hiromitsu Asai and Yuichi Kawamura
NTT Opto-electronics Laboratories, 3-1 Morinosato-Wakamiya, Atsugi, Kanagawa 243-01, Japan
(Received 23 July 1990)

The intersubband absorption in $In_{0.53}Ga_{0.47}As/In_{0.52}Al_{0.48}As$ multiple quantum wells having various well widths, barrier widths, and doping densities is investigated. As the well width increases from 35 to 200 Å, the energies of the absorption peaks decrease from 300 to 100 meV. For a quantum well of 130 Å, two sharp absorption peaks are observed, corresponding to the transitions from the second to the third subbands E_{32} and from the first to the second E_{21}. This well-width dependence of the peak energy is in good agreement with theoretical calculations of the subband structure and the Fermi level. Line broadening with the well width is discussed in terms of one-monolayer fluctuation and the energy spread of minibands. The oscillator strength and the dipole matrix element are also evaluated. The barrier width and doping dependencies of the E_{21} and E_{32} transitions are studied for the 130-Å-well samples. A decrease in the barrier width contributes to line broadening via the energy spread of minibands, while this has no influence on the oscillator strength. Up to the electron density $N_s = 8\times10^{11}$ cm^{-2}, only the E_{21} peak is observed. For N_s above 1.8×10^{12} cm^{-2}, the E_{32} transition is found to be observed. This behavior is in good agreement with the calculation of the Fermi-energy position. In addition, depolarization and many-body effects are also briefly discussed.

I. INTRODUCTION

Over the last decade, advances in growth techniques for ultrathin layers have spurred many experimental studies on the optical properties of multiple quantum wells (MQW's) and on their application to novel devices.[1–5] In general, interest has been focused on band-to-band transitions including excitonic absorptions. Recently, West and Eglash[6] proposed a new aspect for transitions between the quantized states; intersubband transitions from one confined state to higher confined state in the conduction bands.

The intersubband transition in MQW's has been receiving considerable attention because of its novel optical properties, such as large oscillator strength,[6,7] strong nonlinearity,[8–11] and fast relaxation.[12–15] Optical detectors of 10-μm wavelength have been demonstrated as an application of intersubband transition in $GaAs/Al_xGa_{1-x}As$ MQW's.[16–18] There is considerable interest in a shorter-wavelength infrared detector operating at 2–4 μm for future ultralow loss fiber communications systems. However, the absorption in $GaAs/Al_xGa_{1-x}As$ MQW's is limited to wavelengths longer than 5μm due to its small conduction-band discontinuity (ΔE_c). The $In_{0.53}Ga_{0.47}As/In_{0.52}Al_{0.48}As$ heterostructure is a promising candidate for extending the applicable wavelength range of intersubband absorption.[19–25] This is because this heterostructure has large ΔE_c (500 meV) (Ref. 26) compared with $GaAs/Al_xGa_{1-x}As$. In addition, the $In_{0.53}Ga_{0.47}As/In_{0.52}Al_{0.48}As$ has several advantages for other device applications, such as high electron mobility[27] and high tunneling probability.[28,29] Therefore, $In_{0.53}Ga_{0.47}As/In_{0.52}Al_{0.48}As$ heterostructure have the potential to realize new intersubband-absorption devices combining resonant-tunneling effects.

In addition, from the viewpoint of basic physics there has been much interest in intersubband absorption. This is because it gives an experimental solution to finite one-dimensional potential problems.[30] So far, subband levels in quantum wells or band offset ratios in heterostructures have been mainly determined by band-to-band transitions such as photoexcitation and photoluminescence processes.[31–33] Since the band-to-band transitions involve not only electron subbands but also hole subbands, fundamental absorption edges in bulk materials, and excitonic binding energy, there are some ambiguities in the experimental evaluation of subband structures. Especially, the hole subband structure is complicated due to its anisotropy and degeneracy. On the other hand, intersubband absorption reduces to a simple problem because of the transitions only in the conduction bands, and its spectral shape is also simple. Therefore, intersubband absorption can precisely determine subband levels even in more complicated quantum-well structures.

The purpose of this paper is to clarify the subband structure of electrons by studies on intersubband absorption in $In_{0.53}Ga_{0.47}As/In_{0.52}Al_{0.48}As$ MQW's having a wide variety of well widths, barrier widths, and doping levels. The outline of this paper is as follows. The experimental procedure including sample preparation is presented in Sec. II. Section III consists of four subsections describing experimental results and includes discussion. In Sec. III A, the general properties of intersubband transitions are presented. Next the well-width, barrier-width, and doping-level dependencies on the absorption characteristics are studied in Secs. III B, III C, and III D, respectively. One of the remarkable features discussed in

these sections is the observation of two sharp absorption peaks for wide and/or highly doped quantum wells, preliminary results of which have been previously reported.[21–24] The energies of these absorption peaks are compared with subband level calculation, and the Fermi-level position is also discussed. Calculations confirm that these peaks are due to the transitions from the second to the third subband as well as from the first to the second. In addition, depolarization and many-body effects are briefly discussed. Finally the conclusion of this work is given in Sec. IV.

II. EXPERIMENTAL PROCEDURE

The 70-period lattice-matched $In_{0.53}Ga_{0.47}As/In_{0.52}Al_{0.48}As$ MQW's were grown on Fe-doped (001) InP substrates by molecular beam epitaxy (MBE). Prior to growth, the substrate surface was thermally cleaned under the exposure of arsenic vapor, monitoring reflection high-energy electron diffraction. Growth temperature and arsenic vapor pressure during growth were 510 °C and 2×10^{-5} Torr, respectively. Growth rate was 1.2 μm/h. In order to study well-width dependence, the $In_{0.53}Ga_{0.47}As$ well width L_z was varied from 30 to 200 Å under a constant barrier width of 68 Å. On the other hand, the $In_{0.52}Al_{0.48}As$ barrier width L_b was varied from 20 to 130 Å for a fixed well width of 130 Å. Almost all MQW samples were uniformly doped both in the well and barrier with Si atoms at a concentration of $2\times10^{17}-5\times10^{18}$ cm^{-3}. For comparison, MQW's with doped wells or barriers were also prepared. The actual carrier density was determined by van der Pauw measurements. The intersubband absorption was measured by using a Fourier-transform infrared spectrometer. The measurements were mainly performed at Brewster's angle (73°) to maximize the normal component of the electric field vector and to reduce reflection. The specular InP wafer was also measured as the reference sample. For the experiments with polarized light, a KRS-5 wire-grid polarizer was utilized.

III. RESULTS AND DISCUSSION

A. Intersubband-absorption spectra

Figure 1 shows the infrared-absorption spectra measured for a 68-Å-well MQW at 300 K. The sample was oriented at an angle θ with respect to the plane of incidence. It is clear from this figure that a strong absorption peak was observed at $\theta=70°$ while it vanished below $\theta=10°$. This indicates that only a normal component of the electric field contributions to the intersubband transition. The integrated absorption intensity I_A shown in Fig. 2 makes it clearer. For simplicity, the integrated intensity in this study was estimated by simply multiplying the peak absorbance [$=-\log_{10}$(transmittance)] by the full width at half maximum (FWHM) of the absorption spectra (in units of eV). From simple geometric optics, the angular dependence of the absorption intensity is predicted to vary as $\sin^2\alpha/\cos\alpha$, where α is the angle of propagation in the sample relative to the normal to the sample surface and is related to θ by Snell's law

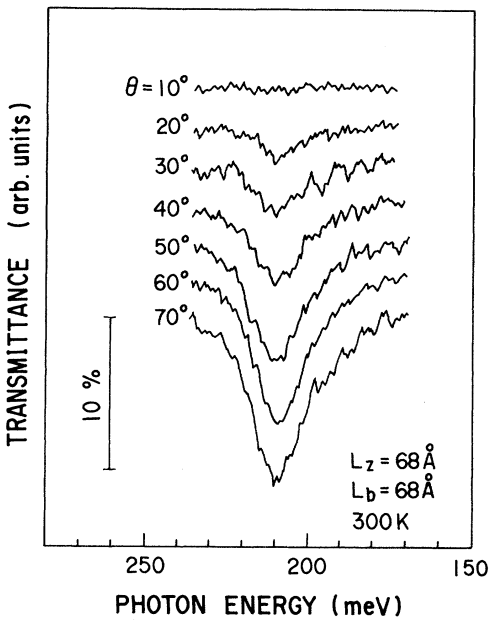

FIG. 1. The intersubband-absorption spectra for a 68-Å-well MQW oriented at an angle θ with respect to the plane of incidence.

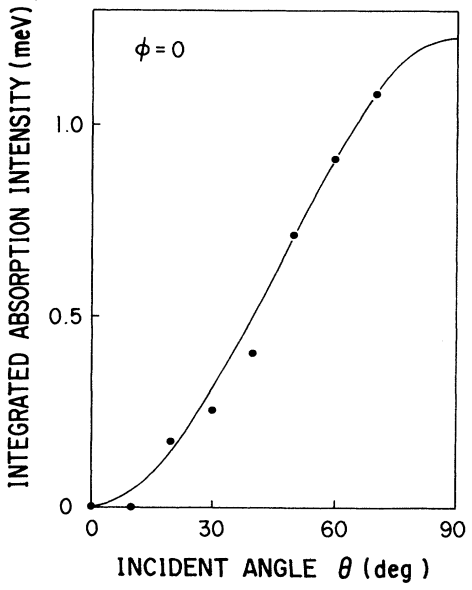

FIG. 2. The integrated absorption intensity as a function of the light incident angle θ. The integrated intensity was estimated by simply multiplying the peak absorbance [$=-\log_{10}$(transmittance)] by the spectral linewidth (FWHM). The solid curve indicates the predicted dependence normalized at $\theta=70°$.

$\sin\alpha=(1/n_r)\sin\theta$. The predicted variation is drawn as a solid curve normalized to the absorption intensity at $\theta=70°$ in Fig. 2, and is in good agreement with the experimental data. In addition, at a Brewster angle of $\theta=73°$ the effect of polarization angles ϕ in the incident light was also measured. The absorption intensity normalized at $\phi=0°$ varied as $\cos^2\phi$, as shown in Fig. 3. The dependence of the absorption on both the light incident angle θ and the polarization angle ϕ provides direct evidence that the observed absorption spectra are due to the intersubband transition.

For the intersubband transition, it is necessary to accumulate electrons in quantized conduction subbands. For this purpose, some authors doped impurities into well layers,[16–18,20,25] while others doped the barrier layers (i.e., modulation doping).[6,13,14,19,30,34] However, there have been no reports directly comparing them. We now investigate the effect of this doping profile difference in MQW's on the absorption spectra. Figure 4 shows the absorption spectra for three MQW's that have doped wells, doped barriers, and a combination of doped wells and barriers. In addition, the experimental data including sheet electron density are presented in Table I. For the sample doped into both the wells and barriers, the absorption intensity was found to be twice as strong as that of the other two samples. Moreover, these two samples indicated comparable absorption intensity. This behavior is directly related to the electron density in quantum wells, and means that all of the Si-donor atoms introduced into the MQW's completely activate and contribute to the two-dimensional electron gas in quantum wells. In addition, there is no difference concerning the spectral linewidth between the doped-well and the doped-barrier samples (16 meV). This suggests that the scattering of ionized impurities in the wells does not actually broaden the absorption spectra.

On the other hand, the absorption peak energy is different among the three samples due to the band-

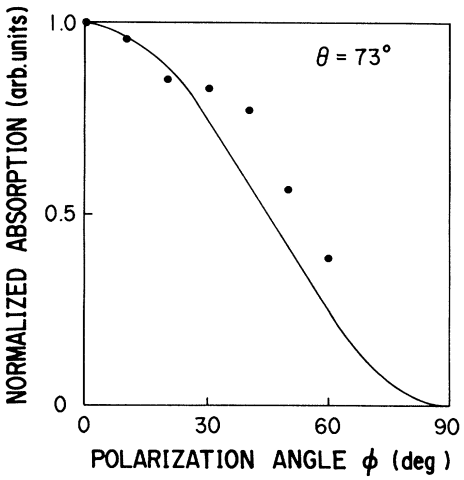

FIG. 3. The normalized absorption intensity of a 68-Å-well MQW oriented at $\theta=73°$ as a function of the polarization angle ϕ. The intensity is normalized at $\phi=0°$. The solid line represents the calculated $\cos^2\phi$ dependence.

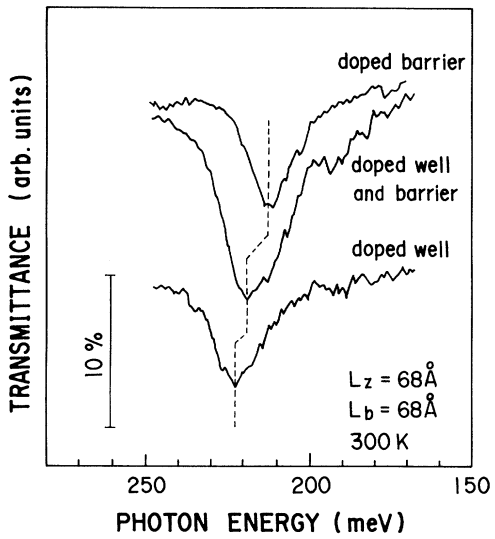

FIG. 4 The intersubband-absorption spectra for 68-Å-well MQW's having doped wells, doped barriers, and a combination of doped wells and barriers.

bending effect,[6,34,35] where the ionized impurities and accumulated electrons modify the potential profile of the quantum well resulting in a change in subband levels. We now briefly discuss this effect. The doped-barrier sample has a convex well bottom and the combination of the doped well and barrier sample also has a weak convex well, while the doped well is concave. In the order of these potential modifications, the intersubband energy shifts to the higher-energy side, as shown in Fig. 4. Furthermore, the sample doped into both the well and barrier is predicted to be closest to the flat-band situation in these samples. In this case, the energy shift was evaluated to be less than the difference (3 meV) between those for the doped well and for the combination of the doped well and barrier. A similar value has also been found in the self-consistent calculation of Schrödinger's equation and Poisson's equation.[6,34,35] To compare the measured absorption energy with the subband-level calculation described later, therefore, we focused on the MQW's doped into both the wells and barriers.

B. Well-width dependence

The well width is one of the key parameters for determining the energy of the intersubband absorption peak.[23] The absorption spectra for the well widths from 35 to 200

TABLE I. Experimental data of the sheet electron density N_s, the absorption peak energy E, the linewidth (FWHM) Γ, and the integrated absorption intensity I_A.

Doped layer	N_s (cm^{-2})	E (meV)	Γ (meV)	I_A (meV)
Well	9.1×10^{11}	221	16.1	0.52
Well and barrier	1.9×10^{12}	218	21.1	1.35
Barrier	8.7×10^{11}	213	16.1	0.61

Å are shown in Fig. 5. As the well width decreased, the absorption peaks shifted to the higher-energy side and the spectral linewidths became wider. Below a well width of 35 Å, no appreciable spectral peak was observed. It is noteworthy that two sharp absorption peaks are observed in a 130-Å-well width, where the absorption energies were 132 and 94 meV, and the linewidths were 12 and 10 meV.

To evaluate experimentally the energy difference between the subband levels, the absorption peak energy is plotted as a function of well width, as shown in Fig. 6. The spectra for a carrier concentration of 1.5×10^{18} cm^{-3} are indicated by solid circles in this figure. The maximum energy obtained in this work was 300 meV, corresponding to a wavelength of 4.1 μm. The peak energy decreased monotonically with an increase in the well width up to 130 Å. At this well width, another peak appeared in the higher-energy side. Subsequent absorption peaks were smoothly connected with the higher-energy peak of the 130-Å-well sample. When the carrier concentration is 4×10^{17} cm^{-3}, the samples above 130-Å width indicated different absorption peaks from those at $n=1.5\times10^{18}$ cm^{-3}. These peak energies are plotted as open circles in Fig. 6. These data were connected smoothly with the lower-energy peak of the 130-Å-well sample.

To determine the subband structure, we performed a calculation for subband energy levels in the finite square potential wells using an envelope-function approximation[36] and taking band nonparabolicity into account.[37] Band-bending, exciton, exchange interaction, and depolarization effects are ignored in this calculation for simplicity. In fact, the band-bending effect is relatively small ($\sim$3 meV), as mentioned in Sec. III A. The exciton effect is the interaction of the excited electron with the hole in the initial state, analogous to the exciton associated with the valence to conduction-band transition. The exciton shift for doped GaAs/$Al_xGa_{1-x}As$ MQW's ($\sim10^{12}$ cm^{-2}) has been reported to be $\sim$3 meV,[35] which is relatively small compared with the exchange interaction and depolarization effects. The exciton shift in our samples is also believed to be a similarly minor effect. The exchange interaction and depolarization effects are very important at the high doping level. Therefore, these effects will be discussed from the viewpoint of the peak shift with doping density in Sec. III D.

The material parameters used in this calculation are as follows: for $In_{0.53}Ga_{0.47}As$, electron effective mass $m^*/m_0=0.042$ and energy band gap $E_g=0.74$ eV, while for $In_{0.52}Al_{0.48}As$, $m^*/m_0=0.075$ and $E_g=1.45$ eV; conduction-band discontinuity $\Delta E_c=0.5$ eV. The non-

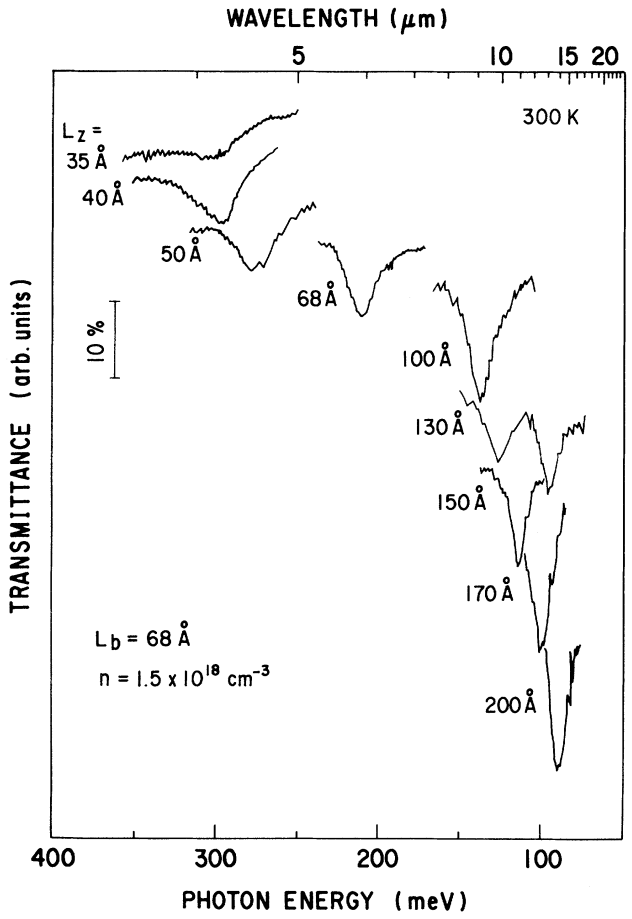

FIG. 5. The intersubband-absorption spectra for uniformly doped MQW's (1.5×10^{18} cm^{-3}) with various well widths.

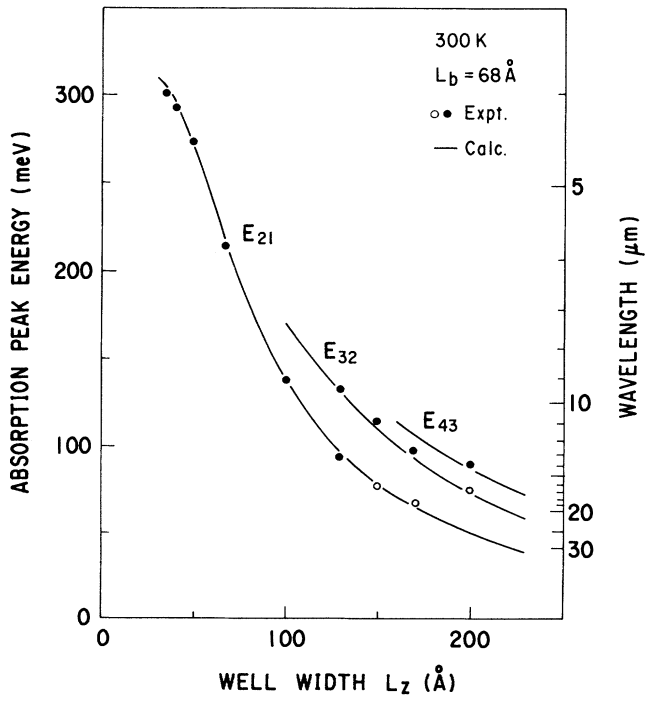

FIG. 6. The absorption peak energy as a function of well width. The solid and open circles indicate the experimental data at doping concentrations of 1.5×10^{18} and 4×10^{17} cm^{-3}, respectively. The lines are the theoretical results of the energy difference between the subband levels, taking into account band nonparabolicity.

parabolicity parameter of $In_{0.53}Ga_{0.47}As$ α is 1.24 eV^{-1}, which is estimated from the following relationship:[37]

$$\alpha=(1-m^*/m_0)^2/E_g \ . \quad (1)$$

The calculated results are also shown as solid curves in Fig. 6. These curves are found to be in good agreement with the experimental data for both the concentrations of 4×10^{17} and 1.5×10^{18} cm^{-3}.

It is clear from Fig. 6 that the higher-energy peak (132 meV) for the 130-Å-well sample corresponds to the transition from the second to the third subbands E_{32}. The energy peaks obtained for wider quantum wells are also due to the transitions between the higher-order subbands. For example, the 89-meV energy peak in a 200-Å well is attributed to absorption from the third to the fourth subbands E_{43}.

On the basis of our calculations, the second subband level just reaches the top of the barrier at a width of 35 Å. Below this width, it should be pushed up into the continuum states. In this circumstance, optical transition occurs between the bound state in the quantum well and the extended continuum states above the top of the barrier. Therefore, the peak energy shift with a decreasing well width saturates around 35 Å.

Intersubband absorption reflects not only the difference between the subband energies but also the position of the Fermi level relative to the subband structure. Figure 7 shows calculated subband and Fermi levels as a function of well width. The Fermi level was calculated for carrier concentrations of 1.5×10^{18} and 4×10^{17} cm^{-3}. For a constant doping level of 1.5×10^{18} cm^{-3}, as the well width increases, the higher-order subbands also cross the Fermi level. Above a width of 110 Å, electrons begin to populate the second subband and make the E_{32} transition possible. The E_{21} transition from the first to the second subband also occurs at large k_x or k_y, although the final empty state density in the second subband is reduced (see the inset in Fig. 7). For $n=4\times10^{17}$ cm^{-3}, however, no electron populates the second subband for a well width up to 180 Å. In this case, the absorption peaks are due only to the E_{21} transition. The above discussion is consistent with the assignment of absorption peaks determined by the subband-level calculation (see Fig. 6). In this way, we can determine the transition levels for all the absorption peaks observed in this study.

Figure 8 shows spectral linewidth as a function of well width. The linewidth of the E_{32} transition was slightly larger than that for the E_{21} spectrum. As the well width decreased, the linewidth of the E_{21} transition became wider up to 32 meV. A similar magnitude and well-width dependence of the spectral linewidth has also been found in modulation-doped $GaAs/Al_xGa_{1-x}As$ MQW's.[13]

We now turn to discussions of the linewidth of the intersubband transitions and its well-width dependence. The linewidth is determined by several mechanisms.[19,38]

(i) The intersubband scattering time τ at the upper subband leads to a spectral width that is proportional to $1/\tau$. The scattering time is mainly dominated by the interaction with the longitudinal-optical (LO) phonon when the transition energy is greater than LO-phonon energy. The

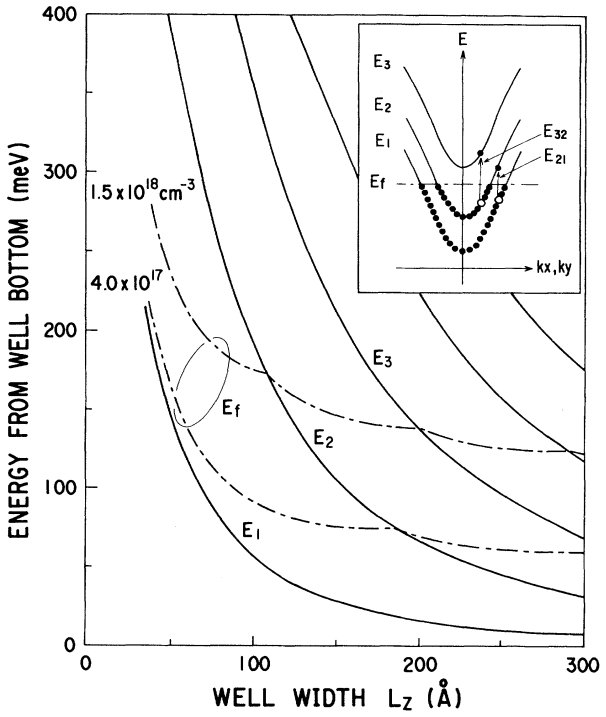

FIG. 7. The calculated subband energy and Fermi level at carrier concentrations of 1.5×10^{18} and 4×10^{17} cm^{-3} as a function of the well width. The inset indicates the schematic subband structure.

intersubband scattering time due to LO phonons has been evaluated experimentally by many authors.[12–15] According to these reports, the scattering time is in the range of 1–10 ps. This lifetime range corresponds to the spectral linewidth of 0.14–1.4 meV, which is very small compared with our experimental data. In addition, the prob-

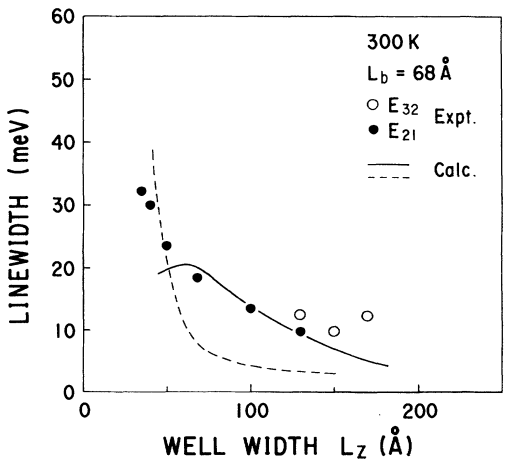

FIG. 8. The spectral linewidth (FWHM) as a function of the well width. The solid and open circles represent the data for the E_{21} and E_{32} transitions, respectively. The solid and dashed lines indicate the calculated line broadening caused by the structural inhomogeneity of the one-monolayer fluctuation and by the energy spread of minibands, respectively.

ability of the LO-phonon interaction is theoretically predicted to decrease with a decrease in the well width.[39,40] This prediction is inconsistent with the well-width dependence of the linewidth in our experiment. Although the intersubband scattering time is one of the most important parameters dominating the dynamics of photoexcited electrons, it cannot be directly projected onto the spectral linewidth. Therefore, the scattering time was ignored in our discussion concerning linewidth.

(ii) The nonparabolicity of the conduction band causes different transition energies in different regions of the k space and a concomitant broadening of the spectral line. Since the nonparabolicity in the $In_{0.53}Ga_{0.47}As$ conduction band is large, the difference in the transition energies at $k=0$ and $k=k_f$ cannot be ignored.[19,38] However, the nonparabolicity parameter [α in Eq. (1)] decreases with an increase in the energy of the subband states.[38] As a result, the broadening of the linewidth due to this effect should decrease with a decreasing well width, which is inconsistent with our well-width dependence. This effect plays a role in the doping dependence of the linewidth.

(iii) The exchange interaction among electrons in the ground subband[41,42] causes different energy lowering of subband states at $k=0$ and $k=k_f$ and results in line broadening. However, the exchange interaction effect is insensitive to well-width variation.[41] This effect will explain the doping dependence of the spectral broadening.

(iv) The miniband due to interaction among the adjacent wells leads to the energy spread of a transition level. Since the subband energy increases with a decrease in well width, the energy spread of the miniband becomes larger, resulting in a spectral broadening with a decrease in the well width. In addition, this effect is especially dominant with respect to an increase in the linewidth for a narrower barrier-width sample, as will be described in Sec. III C.

(v) The inhomogeneities of layer thickness and composition influence the energy of the electronic states and result in a distribution of various transition energies of the intersubband absorption. This effect becomes relatively larger as the well width decreases.

From the above discussion, the spectral broadening with a decrease in the well width is found to be attributed mainly to the energy spread of the miniband and the inhomogeneities of layer thickness. Assuming that the miniband spread yields simply the spectral broadening, the linewidth can be estimated roughly from the Kronig-Penney calculation. Furthermore, if there is a one-monolayer fluctuation of $\pm a_0/2$ (± 2.9 Å) for the well width in our samples, the broadening due to the structural inhomogeneity can also be predicted. These calculated results are drawn as solid and dashed lines in Fig. 8. Note that the value of 3 meV is added to these theoretical curves as a well-width-independent component. This value corresponds to the contribution due to the nonparabolicity effect, as described in Sec. III D. These curves are found to be in good agreement with the experimental data. In a wide-well region, the linewidth is mainly determined by the one-monolayer fluctuation in the well width, while in narrow wells the line broadening is attributed to the energy spread of the excited miniband.

Finally we discuss the integrated absorption intensity and the oscillator strength of the intersubband transitions. Figure 9 shows the integrated absorption intensity as a function of the well width. The integrated intensity was estimated by simply multiplying the peak absorbance [$=-\log_{10}$(transmittance)] by the spectral linewidth (FWHM). Therefore, note that these intensities are underestimated compared with the absorbance integrated over the photon energy. As the well width increased, the absorption intensity of the E_{21} transition increased steeply up to a width of 40 Å, and then increased gradually. Subsequently, the E_{21} intensity decreased rapidly at a 130-Å-well width, and simultaneously the E_{32} transition appeared and increased. The reduction in the E_{21} intensity at 130 Å is attributed to the electron population in the second subband, which leads to both the decrease in the electron density of the E_1 subband and the decrease in the corresponding empty-state density of the E_2 subband.

For wide quantum wells above 130 Å, therefore, the E_{21} and E_{32} intensities must be discussed as related to the sheet carrier densities in the first subband N_{s1} and in the second subband N_{s2}. The N_{s1} and N_{s2} can be evaluated from the following equation:

$$N_s = N_{s1} + N_{s2} = \frac{m^*}{\pi\hbar^2}(E_f - E_1) + \frac{m^*}{\pi\hbar^2}(E_f - E_2) , \quad (2)$$

where m^* is the $In_{0.53}Ga_{0.47}As$ effective mass ($m^*/m_0 = 0.042$), $\hbar$ indicates Plank's constant, E_f is the Fermi energy, and E_1 and E_2 are the energies of the first and second subband. In the parameters of Eq. (2), total

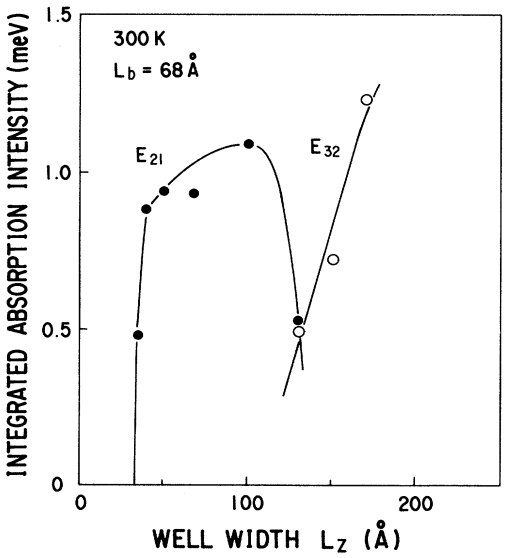

FIG. 9. The integrated absorption intensity as a function of the well width. The integrated intensity was estimated by simply multiplying the peak absorbance [$=-\log_{10}$(transmittance)] by the spectral linewidth (FWHM). The solid and open circles represent the data for the E_{21} and E_{32} transitions, respectively. The solid lines are drawn through the points as a guide.

N_s is measurable by the van der Pauw method and the E_1 and E_2 subband energies have been indicated in Fig. 7. Since E_f is deduced from Eq. (2). N_{s1} and N_{s2} can be estimated individually.

From this calculation of N_{s1} and N_{s2} and from the experimental data of the integrated absorption intensity I_A at carrier concentrations of 4×10^{17} and 1.5×10^{18} cm^{-3}, we can obtain individually the oscillator strength for the E_{21} and E_{32} transitions. In the case of light incidence at the Brewster angle, the dipole matrix element $\langle z \rangle$ and the oscillator strength f of the intersubband transition are given by[6]

$$f \equiv 4\pi m^* \omega \langle z \rangle^2 / h \tag{3}$$

and

$$I_A = N_s W \frac{e^2 h}{4\epsilon_0 m^* c} \frac{f}{n_r^2 (n_r^2+1)^{1/2}} , \tag{4}$$

where ω is the transition frequency (i.e., the peak frequency in the absorption spectrum), W is the number of wells ($W=70$), n_r is the refractive index of $In_{0.52}Ga_{0.48}As$ ($n_r=3.6$), and N_s is the sheet carrier density in each subband. Note that we have used m^* in these equations rather than the free-electron mass m_0, in order to compare with the values reported by Levine *et al.*[20] Substituting measured values of I_A into Eqs. (3) and (4), f and $\langle z \rangle$ were obtained for samples of 35–200 Å.

Figure 10 shows f_{21} and f_{32} as a function of the well width. It is found that f_{21} is in the range of 0.2–0.35 and is almost independent of the well width, while f_{32} is 0.55–0.75. These values are slightly smaller than the previous data,[19,20] because of the underestimation of the integrated absorption intensity. It is noteworthy that f_{32} is about 2.5 times stronger than f_{21}. The dipole matrix element $\langle z \rangle$ is shown in Fig. 11. $\langle z_{21} \rangle$ increased from 8 to 17 Å as the well width increased from 35 to 170 Å. In the well-width range of 130–200 Å, $\langle z_{32} \rangle$ also increased from 20 to 30 Å, which is slightly larger than $\langle z_{21} \rangle$.

For an electron in a well between two barriers of infinite height and width, the $\langle z_{n+1,n} \rangle$ and $f_{n+1,n}$ of the transition between the nth and $(n+1)$th subband are given by[6]

$$\langle z_{n+1,n} \rangle = L_z \frac{8}{\pi^2} \frac{n(n+1)}{(2n+1)^2} \tag{5}$$

and

$$f_{n+1,n} = \frac{64}{\pi^2} \frac{n^2 (n+1)^2}{(2n+1)^3} , \tag{6}$$

where L_z is the well width. It is found from Eq. (6) that f_{21} and f_{32} are 0.96 and 1.87, respectively, which are independent of the well width. In addition, the f_{32}/f_{21} ratio of 1.94 calculated from Eq. (6) is close to our value of 2.5.

The $\langle z_{21} \rangle$ and $\langle z_{32} \rangle$ obtained from Eq. (5) are drawn as dashed lines in Fig. 11. The $\langle z_{21} \rangle$ calculated for finite barrier height by Levine *et al.*[20] is also shown as a solid line in this figure. It is noteworthy that these three calculated curves of $\langle z_{21} \rangle$ and $\langle z_{32} \rangle$ indicate a similar depen-

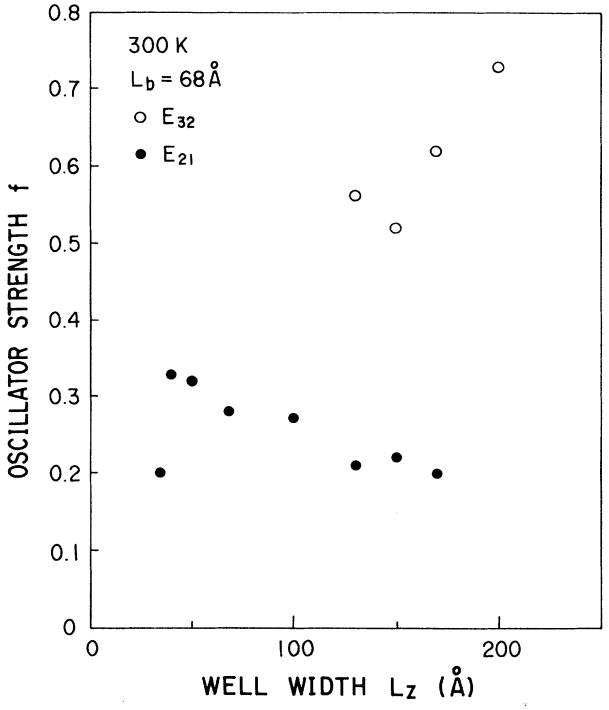

FIG. 10. The oscillator strength as a function of the well width. The solid and open circles represent the data for the E_{21} and E_{32} transitions, respectively.

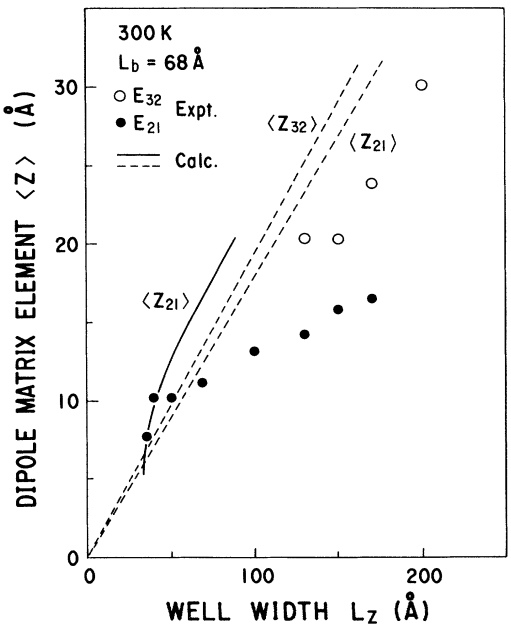

FIG. 11. The dipole matrix element as a function of the well width. The solid and open circles represent the data for the E_{21} and E_{32} transitions, respectively. The dashed lines are the theoretical predictions for the simple model of the infinite barrier height (see text). The solid line is Levine's calculation for the finite barrier height (Ref. 20).

dence on the well width. The experimental data are in good agreement with the calculation in the range of narrow-well widths, but they deviate to the small side in the wide-well region.

A remarkable feature in this section is to observe the two sharp absorption peaks for 130-Å-well samples at $n=1.5\times10^{18}$ cm^{-3}. These absorptions occur as a result of the contribution of three subband levels and their properties are very sensitive to the structure of MQW's. Therefore, we focus on the 130-Å-well MQW's for the investigations of barrier-width and doping dependencies as described below.

C. Barrier-width dependence

Figure 12 shows absorption spectra of various barrier widths in a constant well width of 130 Å. Note that in these samples only well layers were doped to unchange the sheet electron density ($N_s=2\times10^{12}$ cm^{-2}). Therefore we can examine the barrier-width dependence of the absorption intensity independently of N_s. It is clear from Fig. 12 that the observed spectra consist of two absorption peaks. As described in the preceding subsection, the peak at the higher-energy side corresponds to the E_{32} transition, while the lower-energy peak is the E_{21} absorption. It is found that the peak energies of both the E_{32} and E_{21} absorption remain with respect to the barrier width. For barrier widths below 25 Å, the E_{32} peak at the higher-energy side disappears completely and simultaneously the E_{21} spectra broaden steeply.

In order to clarify this, the spectral linewidth is plotted in Fig. 13. It is found from this figure that the linewidth variation with the barrier widths is divided into two components. One is the barrier-width-independent component in the range of wide barrier widths. The other is the barrier-dependent component in the narrow region. The former component in the linewidth is believed to be mainly due to the structural inhomogeneity of the one-monolayer fluctuation, as discussed in Sec. III B.

The barrier-width-dependent component in the linewidth broadening is considered to be due to the energy spread of the minibands by the interaction among the adjacent wells. The energy widths of the minibands can be calculated by the Kronig-Penney model taking band nonparabolicity into account. Assuming that the linewidths are described by the simple sum of the miniband widths of the initial and final subbands, the predicted variation of the broadening is indicated by dashed lines in Fig. 13, which is adjusted at a value of $L_b=130$ Å. However, the experimental data were narrow in comparison to the calculation of the total miniband widths.

This reason is explained by electron distribution in the E-k_z space, where the Fermi level lies within the E_2 miniband, as shown in the inset of Fig. 13. The linewidth of the E_{32} transition is given by the energy width of the electron distribution in the initial E_2 band and the corresponding width of the final empty E_3 band. The E_{21} linewidth consists of the energy width of the final empty E_2 band and the corresponding initial E_1 bandwidth. The energy position of the Fermi level can be calculated by substituting N_s (2×10^{12} cm^{-2}), E_1 (38 meV), and E_2

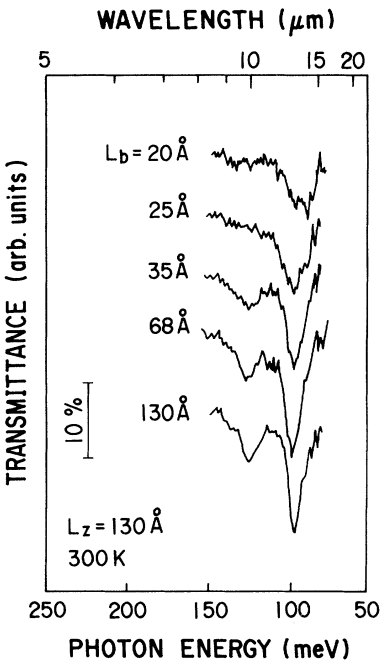

FIG. 12. The barrier-width dependence of the intersubband-absorption spectra for 130-Å-well MQW's.

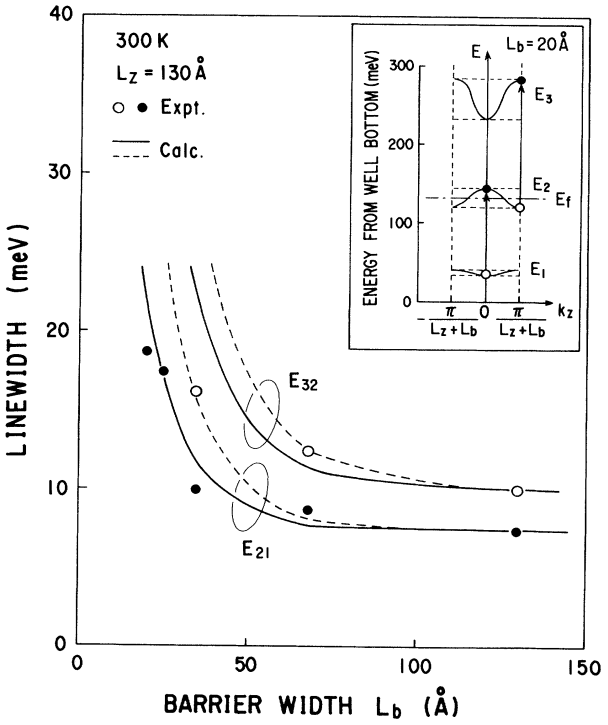

FIG. 13. The spectral linewidth (FWHM) as a function of the barrier width. The solid and open circles represent the data for the E_{21} and E_{32} transitions, respectively. The dashed and solid curves indicate the calculated dependence described by the simple sum of miniband widths and half of the simple sum (see text). The inset displays the schematic subband structure of the MQW with $L_z=130$ Å, $L_b=20$ Å, and $N_s=2\times10^{12}$ cm^{-2}.

(135 meV) into Eq. (2). The E_f is estimated to be 137 meV and lies near the center of the E_2 miniband. In this case half of the simple sum of energy widths in the initial and final minibands is considered to contribute to the spectral linewidth. This result is indicated by solid lines in Fig. 13. The agreement with the experimental data is better than the simple sum of miniband widths.

Figure 14 shows the integrated absorption intensity as a function of the barrier width. It is clear from this figure that the absorption intensity remains almost constant for the barrier-width variation. This means that the oscillator strength and dipole matrix element are independent of the barrier width. This property is very attractive from the viewpoint of device applications. This is because photoexcited electrons can move in a miniband perpendicular to quantum wells without any reduction in the absorption intensity. Similar characteristics have been found in bound-to-continuum transitions and have also been applied to infrared detectors.[17,18]

D. Doping dependence

The doping level can easily vary the Fermi level in quantum wells and has a strong influence on intersubband transitions.[24] Figure 15 shows the dependence of intersubband-absorption spectra on the sheet electron density N_s for a constant well width of 130 Å. In this figure, the higher-energy peak corresponds to the E_{32} transition, while the lower-energy peak is the E_{21} absorption, as discussed in Sec. III B. Up to 8×10^{11} cm^{-2}, only the E_{21} peak was observed around 95 meV. Above $N_s=1.8\times10^{12}$ cm^{-2}, the E_{32} absorption also appeared at 122 meV. Subsequently, the peak shifted gradually toward the higher-energy side and its absorption intensity increased with the doping level.

In order to clarify this behavior, the energies of the E_{21} and E_{32} absorption peaks for 130-Å-well MQW's are plotted as a function of N_s in Fig. 16. Data of 68-Å-well samples are also displayed in this figure. It is clear that the absorption peaks increased gradually with increasing N_s, even for a constant well width. The reason for this peak energy shift is still not fully understood, but some explanations are possible.

One is the depolarization effect due to the electron plasma.[35,43–46] This effect is caused by resonant screening of the infrared field with electrons in quantum wells. As pointed out by Allen *et al.*,[43] the screening of the infrared field shifts the resonant frequency $\omega_{\rm res}$, at which absorption occurs, from the subband-splitting frequency ω_0. In addition, the frequency shift increases with the sheet electron density.

The resonant frequency $\omega_{\rm res}$ is given by the following relationship:[43,44]

$$\omega_{\rm res}^2=\omega_0^2+f\omega_p^2 \tag{7}$$

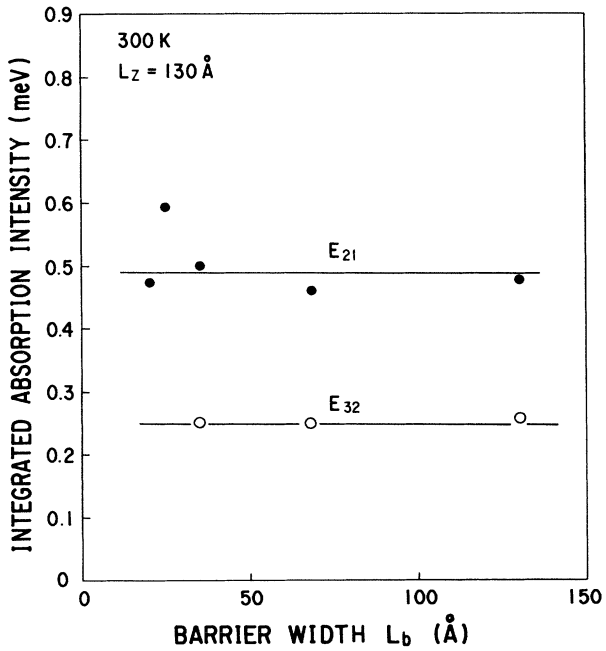

FIG. 14. The integrated absorption intensity as a function of the barrier width. The integrated intensity was estimated by simply multiplying the peak absorbance [$=-\log_{10}$(transmittance)] by the spectral linewidth (FWHM). The solid and open circles represent the data for the E_{21} and E_{32} transitions, respectively. The solid lines are drawn through the points as a guide.

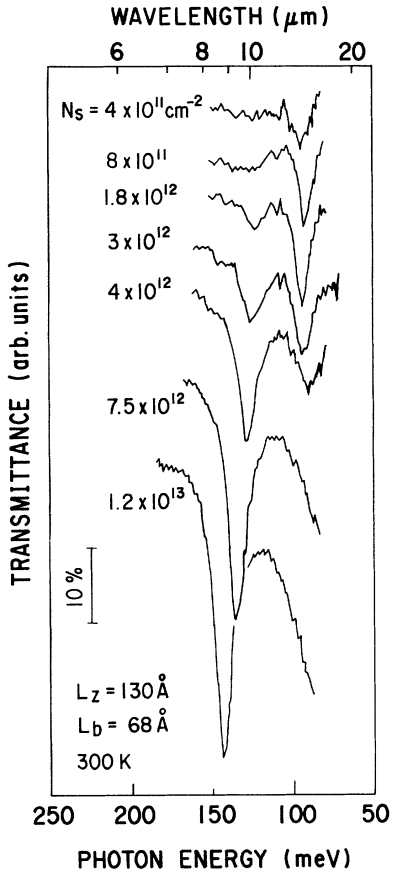

FIG. 15. The doping dependence of the intersubband absorption spectra for 130-Å-well MQW's.

and

$$\omega_p^2 = \frac{N_s e^2}{\epsilon_0 \epsilon m^* L_z} , \tag{8}$$

where ω_p is the plasma frequency, f is the transition oscillator strength, ϵ is the dielectric constant of the well ($\epsilon=10.9$), and m^* is the $In_{0.53}Ga_{0.47}As$ effective mass ($m^*/m_0=0.042$). Note that N_s for each subband (N_{s1} and N_{s2}) derived from Eq. (2) must be used in Eq. (8) instead of the total N_s, when electrons populate the second subband. The oscillator strengths for the E_{21} and E_{32} transitions (f_{21} and f_{32}) have been indicated in Fig. 10. As a result, using Eqs. (7) and (8), we can obtained the peak energy shift by the depolarization effect, which is indicated by solid lines in Fig. 16. These curves are found to be in good agreement with the experimental data.

Another possibilty for the energy shift with N_s is the effect of electron-electron interactions.[41] It has been reported that exchange interactions of electrons in doped quantum wells cause energy lowering on the populated initial-state subbands, while there is no appreciable effect of the exchange interactions on the energies of the empty final-state subbands. Consequently, intersubband transition energies increase with electron density. For example, the energy shift of the E_{32} was roughly estimated to be about 19 meV for the 130-Å-well sample having $N_s=1.1\times10^{13}$ cm^{-2}, corresponding to $N_{s2}=4.3\times10^{12}$ cm^{-2}. For the E_{21} transition at high doping levels, where electrons populate the second subband, the final state should also be lowered by the exchange interaction. As a result, the E_{21} transition is considered to be affected only slightly. However, it is difficult to quantitatively evaluate this effect for both E_{21} and E_{32} transitions.

In this way, the N_s dependence of the E_{32} and E_{21} peak energies can be explained in terms of the depolarization effect and exchange interaction. However, further studies are necessary to clarify this point.

Figure 17 shows the integrated absorption intensity and spectral linewidth as a function of N_s. It is clear from this figure that, over a wide range of N_s, the linewidth of the E_{21} transition was narrow, compared with that of the E_{32} transition. The narrowest linewidth of the E_{21} absorption is 6.2 meV at low N_s and then increases gradually with an increase in N_s, while the linewidth of the E_{32} spectra (12.4 meV) remains constant. The discussion of the spectral linewidth will be described later.

On the other hand, the absorption intensity was strongly affected by N_s. Initially, the absorption intensity of the E_{21} transition increased linearly with an increase in N_s. At an N_s of 1.8×10^{12} cm^{-2}, the E_{21} absorption

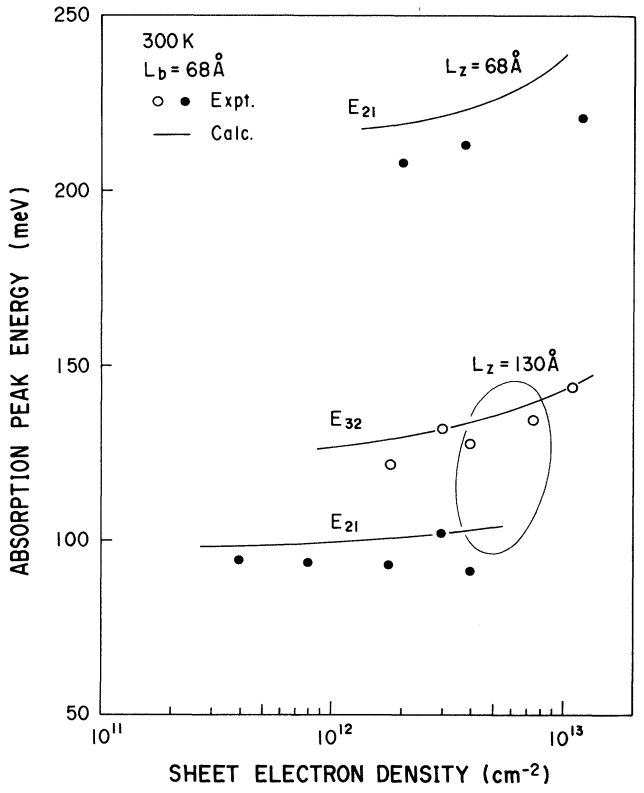

FIG. 16. The absorption peak energy for 130- and 68-Å-well MQW's as a function of the total sheet electron density N_s. The solid and open circles represent the data for the E_{21} and E_{32} transitions, respectively. The solid lines indicate the calculated shift due to the depolarization effect (see text).

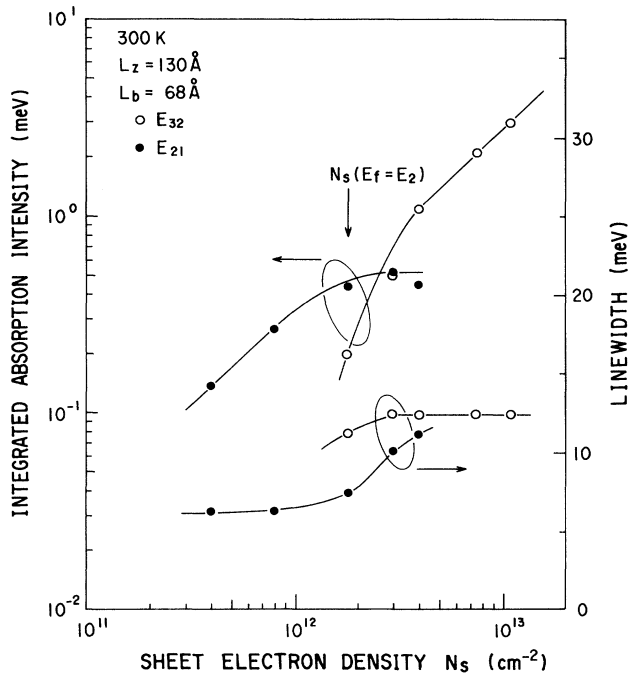

FIG. 17. The integrated absorption intensity and the spectral linewidth (FWHM) as a function of the total sheet electron density N_s. The integrated intensity was estimated by simply multiplying the peak absorbance [$=-\log_{10}$(transmittance)] by the spectral linewidth (FWHM). The solid and open circles represent the data for the E_{21} and E_{32} transitions, respectively. The arrow indicates the calculated N_s where the Fermi level just reaches the second subband E_2. The solid curves are drawn through the points as a guide.

began to saturate, and simultaneously the E_{32} transition appeared. Subsequently, the E_{32} intensity increased steeply with N_s. This suggests that the Fermi level reaches the second subband at $N_s = 1.8 \times 10^{12}$ cm^{-2}. Furthermore, the sheet carrier density at which the E_f reached the second subband was given by substituting E_2 into E_f of Eq. (2) ($E_f = E_2$), and was estimated at 1.9×10^{12} cm^{-2}. This value agrees well with the experimental result ($N_s = 1.8 \times 10^{12}$ cm^{-2}), as indicated by the arrow in Fig. 17.

When the Fermi level reaches the E_2 subband, the E_{21} and E_{32} absorption spectra must be discussed as related to N_{s1} and N_{s2} derived from Eq. (2), instead of total N_s. Figure 18 shows the absorption intensities and spectral linewidth of the E_{21} and E_{32} transitions replotted as functions of N_{s1} and N_{s2}, respectively. It is noteworthy that the E_{32} intensity increases linearly with N_{s2}, in contrast to its variation with N_s shown in Fig. 17. The E_{21} intensity also indicated a linear relationship in the range of the low doping level. These linear relationships allow us to determine the well-defined oscillator strength f for the E_{21} and E_{32} transitions. In the high doping range, however, the E_{21} intensity is not determined by N_{s1}, but by $N_{s1} - N_{s2}$, because the final empty-state density is reduced due to the electron population in the second subband. It was also found from Eq. (2) that $N_{s1} - N_{s2}$ remained at a constant value of 1.9×10^{12} cm^{-2} even though N_{s1} increased above this value. This explains the

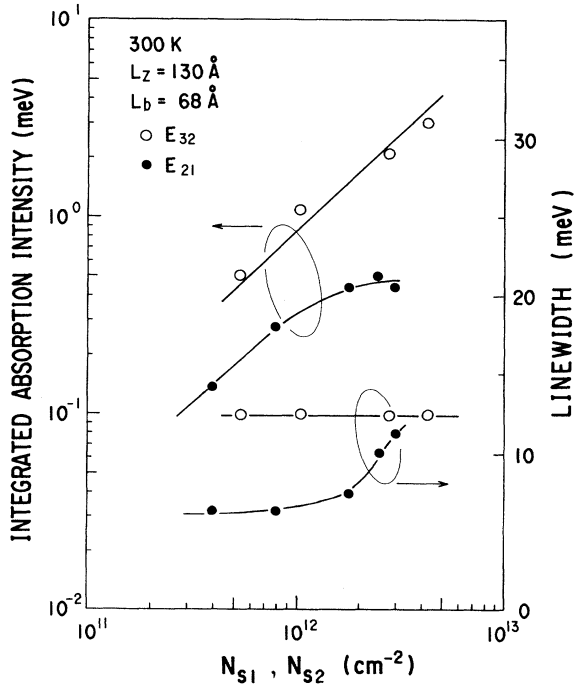

FIG. 18. The integrated absorption intensity and the spectral linewidth (FWHM) replotted with respect to the sheet electron density in the first subband N_{s1} and the second subband N_{s2}. The solid and open circles represent the data for the E_{21} and E_{32} transitions, respectively. The solid curves are drawn through the points as a guide.

saturation in the absorption intensity of the E_{21} transition above $N_s = 1.9 \times 10^{12}$ cm^{-2}, as shown in Fig. 18.

The linewidth variation shown in Fig. 18 consists of the doping-dependent and doping-independent parts. The latter part is attributed to the structural inhomogeneity of the one-monolayer fluctuation and the energy spread of minibands, as discussed in Secs. III B and III C. These contributions were roughly calculated to be 7 and 9.5 meV for the E_{21} and E_{32} transitions, respectively. These values, especially for the E_{21} transition, are in good agreement with the experimental data.

The doping-dependent part is considered to be caused by the effects of band nonparabolicity[38] and the exchange interaction.[41] The nonparabolicity of the conduction band causes different transition energies in different regions of the k space and a concomitant broadening of the spectral line. Since the nonparabolicity in the $In_{0.53}Ga_{0.47}As$ conduction band is large, the difference in the transition energies at $k = 0$ and $k = k_f$ cannot be ignored. The nonparabolicity parameter decreases with an increase in the energy of the subband states.[38] As a result, the contribution of this effect to the line broadening for the E_{32} transition should be smaller than that for the E_{21} transition, which is qualitatively consistent with our doping dependence. On the other hand, the exchange interaction among electrons in the ground subband causes different energy lowering of subband states at $k = 0$ and $k = k_f$ and results in line broadening. A rough estimation yields 20 meV at $N_s = 4 \times 10^{12}$ cm^{-2}, which is considerably large compared with the experimental data. It is difficult to quantitatively evaluate these effects because of the uncertainties in the theoretical treatments, such as an energy-dependent band nonparabolicity parameter and the thermal distribution of electrons up to the higher subbands.

IV. CONCLUSION

The intersubband absorption in $In_{0.53}Ga_{0.47}As/In_{0.52}Al_{0.48}As$ multiple quantum wells (MQW's) having various structures grown on (001) InP was investigated. The doping profile difference in MQW's among the doped well, the doped barrier, and a combination of the doped well and barrier was found to have no appreciable influence on the intersubband-absorption spectra. As the well width increased from 35 to 200 Å, the energies of the absorption peaks decreased from 300 to 100 meV. For a quantum well of 130 Å, two sharp absorption peaks were observed, corresponding to the transitions from the second to the third subbands E_{32} and from the first to the second E_{21}. This well-width dependence of the peak energy was in good agreement with theoretical calculations of the subband structure and the Fermi level, taking into account band nonparabolicity. The line broadening with the well width was discussed in terms of the one-monolayer fluctuation and the energy spread of minibands. The oscillator strength and the dipole matrix element were also evaluated using the integrated absorption intensity. It was found that f_{21} was in the range of 0.2–0.35 and was almost independent of the well width, while f_{32} was in the range of 0.55–0.75. The barrier-

width and doping dependencies of the E_{21} and E_{32} transitions were studied for the 130-Å-well samples. A decrease in the barrier width contributes to line broadening via the energy spread of minibands, while this has no influence on the oscillator strength. Up to $N_s = 8 \times 10^{11}$ cm^{-2}, only the E_{21} peak was observed around 95 meV. For an electron density above $N_s = 1.8 \times 10^{12}$ cm^{-2}, the E_{32} transition was observed at 122 meV. This behavior was in good agreement with the calculation of the Fermi-energy position. In addition, depolarization and many-body effects were also briefly discussed.

ACKNOWLEDGMENTS

The authors would like to thank Mitsuru Naganuma, Osamu Mikami, and Takayuki Sugeta for their continuous encouragement.

[1]W. T. Tsang, Appl. Phys. Lett. **39**, 786 (1981).
[2]T. Ishibashi, S. Tarucha, and H. Okamoto, *Proceedings of the International Symposium on GaAs and Related Compounds, Oiso, Japan,* Inst. Phys. Conf. Ser. No. 63 (IOP, Bristol, 1981), p. 587.
[3]D. A. B. Miller, D. S. Chemla, D. J. Eilenberger, P. W. Smith, A. C. Gossard, and W. T. Tsang, Appl. Phys. Lett. **41**, 679 (1982).
[4]E. E. Mendez, G. Bastard, L. L. Chang, L. Esaki, H. Morkoc, and R. Fischer, Phys. Rev. B **26**, 7101 (1982).
[5]D. S. Chemla, T. C. Damen, D. A. B. Miller, A. C. Gossard, and W. Wiegmann, Appl. Phys. Lett. **42**, 864 (1983).
[6]L. C. West and S. J. Eglash, Appl. Phys. Lett. **46**, 1156 (1985).
[7]L. D. L. Brown, M. Jaros, and D. C. Herbert, Phys. Rev. B **40**, 1616 (1989).
[8]S. Y. Yuen, Appl. Phys. Lett. **43**, 813 (1983).
[9]D. Ahn and S. L. Chuang, IEEE J. Quantum Electron. **QE-23**, 2196 (1987).
[10]D. Walrod, S. Y. Auyang, P. A. Wolff, and W. Tsang, Appl. Phys. Lett. **56**, 218 (1990).
[11]E. Rosencher, Ph. Bois, B. Vinter, J. Nagle, and D. Kaplan, Appl. Phys. Lett. **56**, 1822 (1990).
[12]D. Y. Oberli, D. R. Wake, M. V. Klein J. Klem, T. Henderson, and H. Morkoç, Phys. Rev. Lett. **59**, 696 (1987).
[13]A. Seilmeier, H.-J. Hübner, G. Abstreiter, G. Weimann, and W. Schlapp, Phys. Rev. Lett. **59**, 1345 (1987).
[14]R. J. Bäuerle, T. Elsaesser, W. Kaiser, H. Lobentanzer, W. Stolz, and K. Ploog, Phys. Rev. B **38**, 4307 (1988).
[15]M. C. Tatham, J. F. Ryan, and C. T. Foxon, Phys. Rev. Lett. **63**, 1637 (1989).
[16]B. F. Levine, K. K. Choi, C. G. Bethea, J. Walker, and R. J. Malik, Appl. Phys. Lett. **50**, 1092 (1987).
[17]B. F. Levine, C. G. Bethea, K. K. Choi, J. Walker, and R. J. Malik, J. Appl. Phys. **64**, 1591 (1988).
[18]B. F. Levine, C. G. Bethea, G. Hasnain, V. O. Shen, E. Pelve, R. R. Abbott, and S. J. Hsieh, Appl. Phys. Lett. **56**, 851 (1990).
[19]H. Lobentanzer, W. König, W. Stolz, K. Ploog, T. Elsaesser, and R. J. Bäuerle, Appl. Phys. Lett. **53**, 571 (1988).
[20]B. F. Levine, A. Y. Cho, J. Walker, R. J. Malik, D. A. Kleinman, and D. L. Sivco, Appl. Phys. Lett. **52**, 1481 (1988).
[21]H. Asai, Y. Kawamura, O. Mikami, and M. Naganuma, *Proceedings of the International Symposium on GaAs and Related Compounds, Karuizawa, Japan,* Inst. Phys. Conf. Ser. No. 106 (IOP, Bristol, 1989), p. 393.
[22]H. Asai and Y. Kawamura, Appl. Phys. Lett. **56**, 746 (1990).
[23]H. Asai and Y. Kawamura, Appl. Phys. Lett. **56**, 1149 (1990).
[24]H. Asai and Y. Kawamura, Appl. Phys. Lett. **56**, 1427 (1990).
[25]G. Hasnain, B. F. Levine, D. L. Sivco, and A. Y. Cho, Appl. Phys. Lett. **56**, 770 (1990).
[26]R. People, K. W. Wecht, K. Alavi, and A. Y. Cho, Appl. Phys. Lett. **43**, 118 (1983).
[27]H. Hirose, K. Ohata, T. Mizutani, T. Itoh, and M. Ogawa, *Proceedings of the International Symposium on GaAs and Related Compounds, Karuizawa, Japan,* Inst. Phys. Conf. Ser. No. 79 (IOP, Bristol, 1985), p. 529.
[28]Y. Sugiyama, T. Inata, S. Muto, Y. Nakata, and S. Hiyamizu, Appl. Phys. Lett. **52**, 314 (1988).
[29]Y. Kawamura, H. Asai, K. Wakita, O. Mikami, and M. Naganuma, Jpn. J. Appl. Phys. **28**, L1104 (1989).
[30]M. Nakayama, H. Kuwahara, H. Kato, and K. Kubata, Appl. Phys. Lett. **51**, 1741 (1987).
[31]R. Dingle, W. Wiegmann, and C. H. Henry, Phys. Rev. Lett. **33**, 827 (1974).
[32]R. Dingle, A. C. Gossard, and W. Wiegmann, Phys. Rev. Lett. **34**, 1327 (1975).
[33]R. C. Miller, A. C. Gossard, D. A. Kleinman, and O. Munteanu, Phys. Rev. B **29**, 3740 (1984).
[34]M. J. Kane, M. T. Emeny, N. Apsley, C. R. Whitehouse, and D. Lee, Superlatt. Microstruct. **5**, 587 (1989).
[35]W. L. Bloss, J. Appl. Phys. **66**, 3639 (1989).
[36]G. Bastard, Phys. Rev. B **24**, 5693 (1981).
[37]A. Raymond, J. L. Robert, and C. Bernard, J. Phys. C **12**, 2289 (1979).
[38]R. J. Bäuerle, T. Elsaesser, H. Lobentanzer, W. Stolz, and K. Ploog, Phys. Rev. B **40**, 10 002 (1989).
[39]R. Ferreira and G. Bastard, Phys. Rev. B **40**, 1074 (1989).
[40]S. Rudin and T. L. Reinecke, Phys. Rev. B **41**, 7713 (1990).
[41]K. M. S. V. Bandara, D. D. Coon, Byunsung O, Y. F. Lin, and M. H. Francombe, Appl. Phys. Lett. **53**, 1931 (1988); **55**, 206(E) (1989).
[42]T. Ando, Surf. Sci. **73**, 1 (1978).
[43]S. J. Allen, Jr., D. C. Tsui, and B. Vinter, Solid State Commun. **20**, 425 (1976).
[44]B. D. McCombe, R. T. Holm, and D. E. Schafer, Solid State Commun. **32**, 603 (1979).
[45]A. Pinczuk, S. Schmitt-Rink, G. Danan, J. P. Valladares, L. N. Pfeiffer, and K. W. West, Phys. Rev. Lett. **63**, 1633 (1989).
[46]M. Ramsteiner, J. D. Ralston, P. Koidl, B. Dischler, H. Biebl, J. Wagner, and H. Ennen, J. Appl. Phys. **67**, 3900 (1990).